NATIONAL AERONAUTICS AND SPACE ADMINISTRATION

*Technical Report 32-1393*

# *A Martian Entry Propagation Study*

*John D. Norgard*



JET PROPULSION LABORATORY
CALIFORNIA INSTITUTE OF TECHNOLOGY
PASADENA, CALIFORNIA

June 15, 1969

NATIONAL AERONAUTICS AND SPACE ADMINISTRATION

*Technical Report 32-1393*

# *A Martian Entry Propagation Study*

*John D. Norgard*

**JET PROPULSION LABORATORY**
CALIFORNIA INSTITUTE OF TECHNOLOGY
PASADENA, CALIFORNIA

June 15, 1969

Prepared Under Contract No. NAS 7-100
National Aeronautics and Space Administration

# Preface

The work described in this report was performed by the Telecommunications Division of the Jet Propulsion Laboratory.

# Contents



## Tables



## Figures

## Contents (contd)

### Figures (contd)

## Abstract

In this preliminary study of plasma effects on high-frequency electromagnetic wave propagation, the electromagnetic interaction with the shock-induced plasma flow field generated around a blunt body capsule as it encounters the planetary atmosphere of Mars is examined.

From two mathematical models of the Martian atmosphere (VM-4 and VM-8) and the entry-trajectory characteristics of the capsule, it appears that the communication links to and from the capsule will be blacked out during entry because of the free electron concentration in the wake region of the capsule.

Estimates of the free electron concentration in the wake region indicate peak values of approximately $8 \times 10^{11}$ $e^-$/cc for the VM-4 model atmosphere and peak values of approximately $8 \times 10^{10}$ $e^-$/cc for the VM-8 model atmosphere. Both of these values are above the critical electron concentrations of $6.53 \times 10^{10}$ $e^-$/cc for S-band transmission at 2.295 GHz and the critical electron concentration of $1.99 \times 10^9$ $e^-$/cc for transmission at 400 Mhz. These frequencies are the transmission frequencies for communication links between the capsule and a relay bus and directly between the capsule and the earth, respectively.

# A Martian Entry Propagation Study

## I. Introduction

Part of the objective of a mission to the planet Mars is to obtain data about the Martian atmosphere and surface conditions.[1] To obtain these data, an instrumented capsule will be soft-landed on the surface of the planet.

As the capsule enters the Martian atmosphere, a resistance to its motion by the atmospheric gases will result in a transfer of energy from the capsule to the gases and a subsequent ionization of the gases. The degree of ionization will depend on the composition and properties of the Martian atmosphere and the entry-trajectory characteristics of the capsule. If the degree of ionization is substantial, a shock-induced envelope of ionized gases will form around the capsule as it descends through the planetary atmosphere.

The envelope of ionized gases surrounding the capsule constitutes a plasma flow field, i.e., a macroscopically neutral ionized gas consisting principally of free electrons, free ions, and neutral particles. One effect of the plasma on electromagnetic wave propagation is an attenuation of the wave, the severity of the attenuation depending largely on the degree of ionization of the gases constituting the plasma. At hypersonic entry velocities, the attenuation can be sufficient to cause total loss of signal, or *blackout*, even at extremely high frequencies.

A preliminary examination of the various models of the Martian atmosphere (Ref. 1) and the entry-trajectory characteristics of the capsule[2] indicates that the signal attenuation will be sufficient to cause blackout during some period of the entry phase of a Mars mission. The objective of this study is to determine the actual degree of signal attenuation or blackout to be expected during entry of a blunt capsule into the Martian atmosphere.

A model to describe the actual plasma environment generated around the capsule as it enters the planetary atmosphere will be developed from two mathematical models of the Martian atmosphere (the VM-4 and VM-8) that have been chosen to represent a reasonable range of expected conditions, and from the entry-trajectory characteristics of the capsule. With the use of the plasma

[1] "Mars '71 Technical Study." Internal document.

[2] "1973 *Voyager* Capsule System Constraints and Required Document." Internal document.

environment model developed for each atmospheric model, the points at which blackout begins and ends will be calculated for 400 MHz and 2.295 GHz. These frequencies are the proposed transmission frequencies for communication links between the capsule and a relay bus, and directly between the capsule and the earth, respectively.[1]

## II. Martian Model Atmospheres

The physical properties of the Martian atmosphere and the variation of these properties with altitude above the Martian surface are not accurately known (Ref. 2). Recent information about the planet has led to the proposal of various model atmospheres. Since it is uncertain which model most accurately describes the actual Martian atmosphere, two model atmospheres, the VM-4 and VM-8, are used to develop two different plasma environment models to describe the actual plasma environment that will be encountered by the capsule as it descends through the planetary atmosphere. The properties of these model atmospheres are given in Table 1.[2]

**Table 1. Properties of two model atmospheres**

| Property | Symbol | Unit | Model | |
|---|---|---|---|---|
| | | | VM-4 | VM-8 |
| Surface pressure | $p_0$ | mbar | 10.0 | 5.0 |
| | | lb/ft$^2$ | 20.0 | 10.4 |
| Surface density | $\rho_0$ | (g/cc) $10^5$ | 2.57 | 1.32 |
| | | (slugs/ft$^3$) $10^5$ | 4.98 | 2.56 |
| Surface temperature | $T_0$ | °K | 200.0 | 200.0 |
| | | °R | 360.0 | 360.0 |
| Stratospheric temperature | $T_s$ | °K | 100.0 | 100.0 |
| | | °R | 180.0 | 180.0 |
| Acceleration of gravity at surface | $g_s$ | cm/s$^2$ | 375.0 | 375.0 |
| | | ft/s$^2$ | 12.3 | 12.3 |
| Composition (percent) | | | | |
| $CO_2$ (by mass) | | | 70.0 | 100.0 |
| $CO_2$ (by volume) | | | 68.0 | 100.0 |
| $N_2$ (by mass) | | | 0.0 | 0.0 |
| $N_2$ (by volume) | | | 0.0 | 0.0 |
| A (by mass) | | | 30.0 | 0.0 |
| A (by volume) | | | 32.0 | 0.0 |
| Molecular weight | $M$ | mol$^{-1}$ | 42.7 | 44.0 |
| Specific heat of mixture | $C_p$ | cal/g°C | 0.1530 | 0.166 |
| Specific heat ratio | $\gamma$ | | 1.43 | 1.37 |
| Adiabatic lapse rate | $\Gamma$ | °K/km | −5.85 | −5.39 |
| | | °R/kft | −3.21 | −2.96 |
| Tropopause altitude | $h_t$ | km | 17.1 | 18.6 |
| | | kft | 56.1 | 61.0 |
| Inverse scale height (stratosphere) | $\beta$ | km$^{-1}$ | 0.193 | 0.199 |
| | | ft$^{-1}$ × $10^5$ | 5.89 | 6.07 |
| Continuous surface wind speed | $\bar{v}$ | ft/s | 155.5 | 220.0 |
| Maximum surface wind speed | $v_{max}$ | ft/s | 390.0 | 556.0 |
| Design vertical wind gradient | $dv/dh$ | ft/s/kft | 2.0 | 2.0 |
| Design gust speed | $v_g$ | ft/s | 150.0 | 200.0 |

In the following, let $h$ denote altitude above the Martian surface. Then, the pressure $p(h)$ of each atmospheric model is given by (Ref. 1)

$$p = p_0 \left(1 + \frac{\Gamma}{T_0} h\right)^{\gamma/(\gamma-1)} \tag{1}$$

for $0 \leq h \leq h_t$, where $p_0$ is the surface pressure, $T_0$ is the surface temperature, $\gamma$ is the specific heat ratio, $\Gamma$ is the adiabatic lapse rate, and $h_t$ is the tropopause altitude, as given in Table 1.

Similarly, the density $\rho(h)$ and the surface density $\rho_0$ of each atmospheric model are related by (Ref. 1)

$$\rho = \rho_0 \left(1 + \frac{\Gamma}{T_0} h\right)^{1/(\gamma-1)} \tag{2}$$

for $0 \leq h \leq h_t$.

Above the tropopause altitude $h_t$, each atmospheric model is assumed to be isothermal at the stratospheric temperature of 100°K. As a consequence of this assumption, the pressure and density of each atmospheric model obey an exponential decay law with altitude of the form (Ref. 3)

$$p = p_s e^{-\beta h} \tag{3}$$

$$\rho = \rho_s e^{-\beta h} \tag{4}$$

for $h > h_t$. The terms $p_s$ and $\rho_s$ are defined by

$$p_s \equiv p_t e^{\beta h_t} \tag{5}$$

$$\rho_s \equiv \rho_t e^{\beta h_t} \tag{6}$$

where $p_t$ and $\rho_t$ are the pressure and density at the tropopause altitude as given by Eqs. (1) and (2), respectively.

Figures 1 and 2 are graphs of pressure vs altitude and density vs altitude for the VM-4 and VM-8 model atmospheres obtained from these equations.

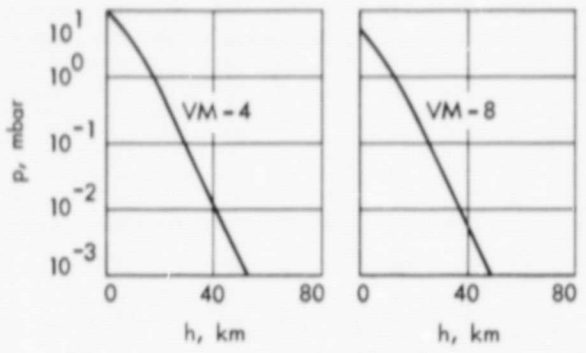


**Fig. 1. Atmospheric pressure vs altitude for two model atmospheres**

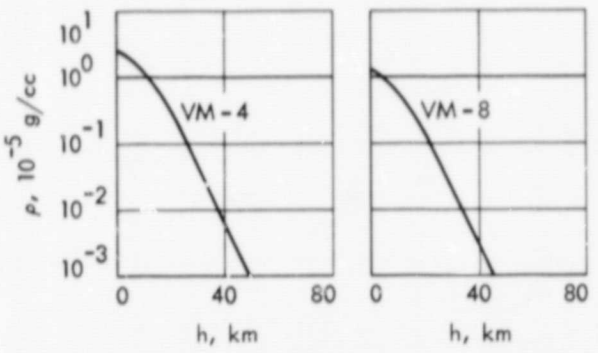


**Fig. 2. Atmospheric density vs altitude for two model atmospheres**

## III. Entry-Trajectory Characteristics

### A. Initial Conditions

The entry phase of a Mars mission will begin at an altitude of 800 kft above the Martian surface. A set of initial conditions consistent with spacecraft approach trajectories, deflection maneuver orientation, and deflection maneuver accuracies is used for the entry-trajectory analysis. These conditions[1] at the entry altitude $h_e$ of 800 kft are (1) entry velocity $v_e$ of 22 kft/s, and (2) entry angle $\psi_e$ of 55 $\pm$6 deg.

### B. Entry-Trajectory Analysis

The approach to the entry-trajectory analysis is to use linear entry-trajectory theory to approximately determine the entry characteristics of the capsule. The entry characteristics of interest in this report are the velocity and elapsed time-from-entry of the capsule calculated as a function of altitude.

The entry-trajectory is assumed to be a straight path at the constant entry angle relative to the local horizontal at the assumed point of entry into the atmosphere. The surface of Mars is assumed to be flat so that the altitude of the capsule above the surface of the planet is independent of the displacement of the capsule from the assumed point of entry into atmosphere (Fig. 3). Clearly, the accuracy of this linear approximation increases with increasing entry angle.

With these simplifying assumptions, the velocity $v(h)$ and the elapsed time-from-entry $\delta t(h)$ of the capsule are given respectively by (Ref. 6)

$$v = v_e e^{-p/2g_s\Delta \sin\psi_e} \tag{7}$$

$$\delta t = \frac{1}{\beta v_e \sin\psi_e}\left[Ei\left(\frac{p}{2g_s\Delta\sin\psi_e}\right) - Ei\left(\frac{p_e}{2g_s\Delta\sin\psi_e}\right)\right] \tag{8}$$

where $p_e$ is the pressure at the entry altitude, $\Delta$ is the ballistic coefficient of the capsule, and $Ei(\zeta)$ is the exponential integral function defined by (Ref. 5)

$$Ei(\zeta) \equiv \int_{-\infty}^{\zeta} d\eta \frac{e^\eta}{\eta}$$

for $\zeta > 0$.

Figures 4 and 5 are graphs of velocity vs altitude and time-from-entry vs altitude for the VM-4 and VM-8 model atmospheres obtained from Eqs. (7) and (8) for an entry velocity of 22 kft/s, an entry angle of 55 deg, and a ballistic coefficient of 0.12 slugs/ft$^2$.

An examination of Fig. 4 reveals that, for the VM-4 model atmosphere, the capsule achieves terminal velocity

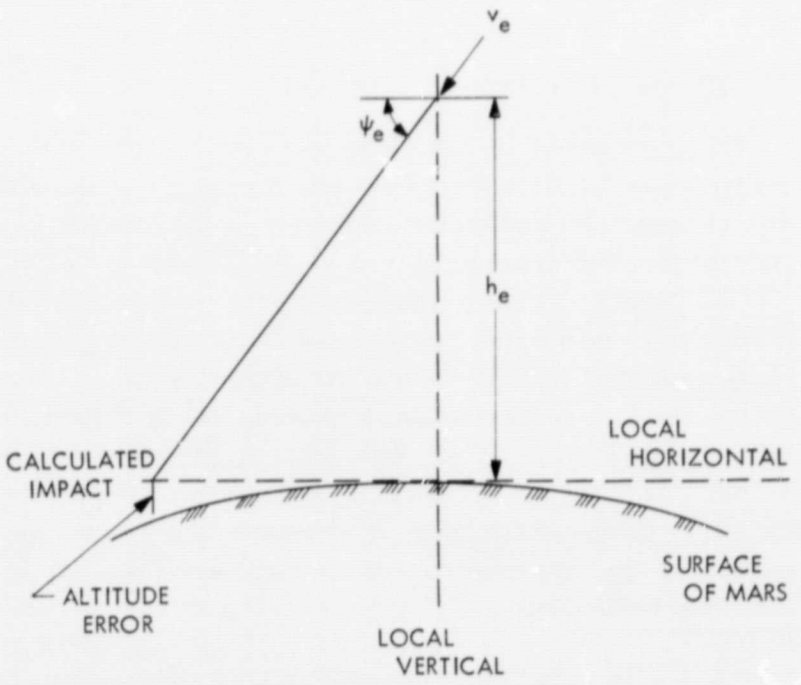


**Fig. 3. Capsule entry-trajectory**

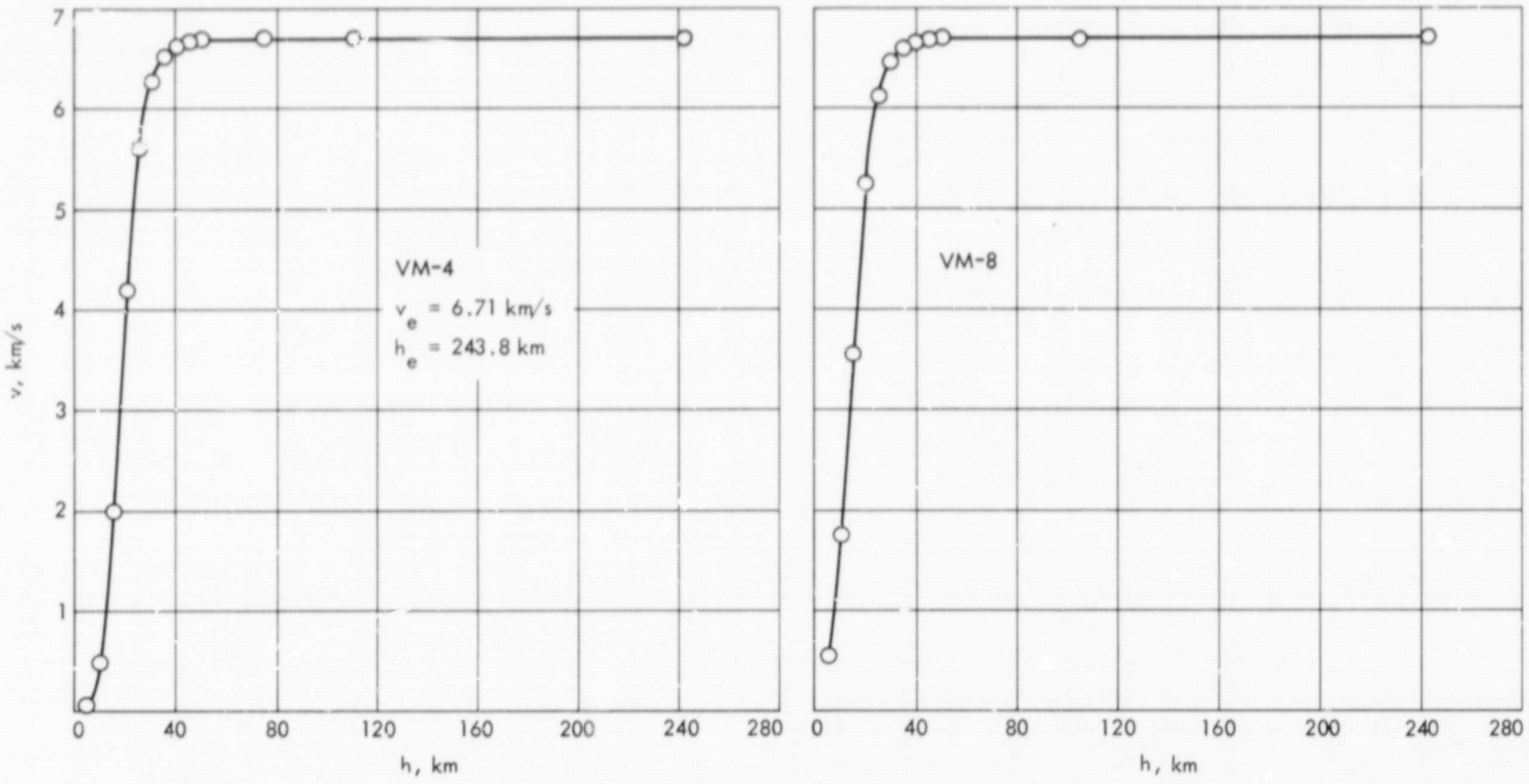


**Fig. 4. Capsule velocity vs altitude for two model atmospheres**

at approximately 50 s after entry. When this condition exists, Eq. (8) is no longer valid and results in the unreasonably high value of 755.0 s to impact. Fortunately, only that part of the graph that lies below 50 s is of interest in the work that follows.

A computer program for the calculation of linear entry-trajectories is described fully in the Appendix.

## IV. Plasma Interaction

The interaction of an electromagnetic wave with a plasma can be described in terms of the parameters of the plasma. The parameters of interest in the present case are the electron concentration and the collision frequency of the plasma. These parameters in turn depend on the interactions of the basic particles constituting the plasma. The number of free electrons contained within the plasma, or the *electron concentration*, is determined by the degree of ionization of the gases constituting the plasma. The number of collisions an electron undergoes per unit time, or the *collision frequency*, is determined by the interaction of the free electrons with ions, neutral particles, and other electrons.

From a knowledge of the spatial and temporal variation of these parameters and a suitably chosen model to represent the plasma, the frequency, permittivity, permeability, and conductivity of the plasma can be determined. The permittivity, permeability, and conductivity describe the macroscopic behavior of the plasma and are called the *constitutive* parameters of the plasma.

The interaction of an electromagnetic wave with the plasma can be determined from the propagation constant of the plasma. The propagation constant is a function of the plasma frequency and the constitutive parameters of the plasma and can be determined either by inverting the dispersion relation or by examining the wave equation in normal form. The real and imaginary parts of the propagation constant contain information about the phase shift and attenuation of the wave as it propagates in the plasma.

The propagation constant of the plasma changes considerably depending on the relationship of the frequency of the electromagnetic wave in the plasma to the frequency of the plasma. For frequencies above the plasma frequency, the plasma behaves as a lossy dielectric, and the electromagnetic wave, while experiencing some attenuation, propagates freely. At frequencies below the plasma frequency, the plasma behaves as a conductor, and the electromagnetic wave is highly attenuated.

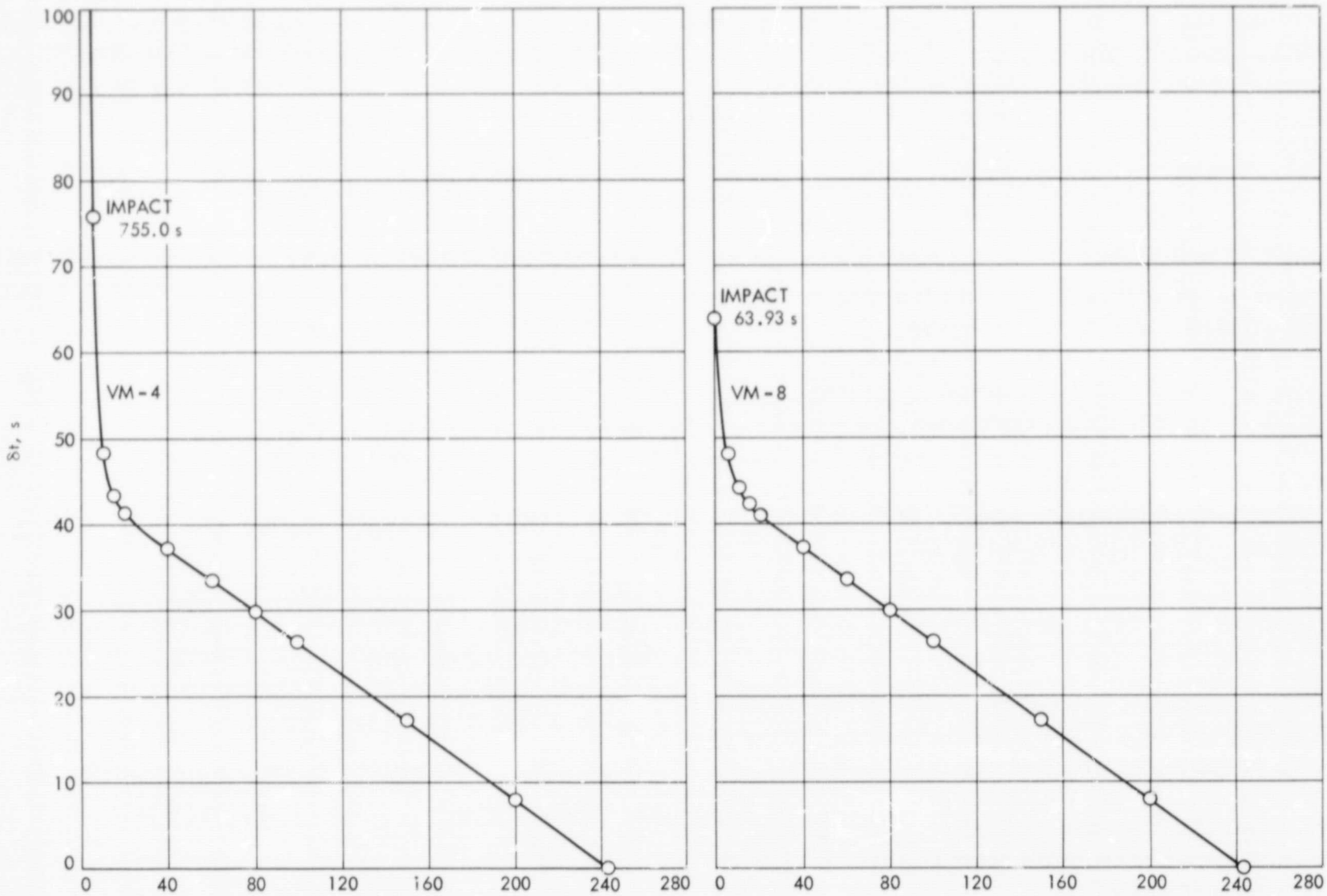


**Fig. 5. Capsule time-from-entry vs altitude for two model atmospheres**

Therefore, the interaction of an electromagnetic wave with the plasma can be determined, in principle, from a study of the relationships between the propagation constant, the constitutive parameters, the plasma frequency, the collision frequency, and the electron concentration of the plasma. In the following sections, these relationships are developed; and, in particular, the propagation constant of the plasma is determined as a function of electron concentration and collision frequency.

### A. Constitutive Parameters of a Plasma

A suitable model of the plasma which is consistent with the limitations of this study is that of a certain number $n$ of electrons per unit volume free to move in an applied electromagnetic field, but subject to a damping force due to collisions characterized by damping constant $\omega_c$. The damping constant $\omega_c$ represents the average number of collisions the electrons undergo per unit time. The macroscopic equation of motion of such electrons is

$$nm\frac{\mathrm{d}\mathbf{v}}{\mathrm{d}t} = nq\left(\mathscr{E} + \mathbf{v}\wedge\mathscr{B}\right) - nm\omega_c\mathbf{v} \tag{9}$$

where the applied electromagnetic field is characterized by the field vectors $\mathscr{E}(\mathbf{r}, t)$ and $\mathscr{B}(\mathbf{r}, t)$. In the present case, the nonlinear $\mathbf{v}\wedge\mathscr{B}$ term is dropped since $|\mathbf{v}\wedge\mathscr{B}| << |\mathscr{E}|$.

In the steady state, with $e^{-i\omega t}$ time-dependence, the equation of motion (9) becomes

$$-i\omega nm\mathbf{v} = nq\mathbf{E} - nm\omega_c\mathbf{v} \tag{10}$$

where the applied electromagnetic field in the steady state is characterized by the single field vector $\mathbf{E}(\mathbf{r})$.

A rigorous derivation of the equation of motion using a statistical distribution function to describe the state of the plasma can be found in Ref. 6.

If the complex electric current density $\mathbf{j}(\mathbf{r})$ and the radian plasma frequency $\omega_p$ are defined by

$$\mathbf{j} \equiv nq\mathbf{v} \tag{11}$$

$$\omega_p^2 \equiv \frac{nq^2}{m\epsilon_0} \tag{12}$$

then with the solution of Eq. (10) for $\mathbf{v}$ and the substitution of the result into Eq. (11), the following relationship between $\mathbf{j}(\mathbf{r})$ and $\mathbf{E}(\mathbf{r})$ can be found:

$$\mathbf{j}(\mathbf{r}) = \frac{\epsilon_0\omega_p^2}{-i\omega + \omega_c}\mathbf{E}(\mathbf{r}) = \left(\frac{\epsilon_0\omega_c\omega_p^2}{\omega^2 + \omega_c^2} + i\omega\frac{\epsilon_0\omega_p^2}{\omega^2 + \omega_c^2}\right)\mathbf{E}(\mathbf{r}) \tag{13}$$

The form of Eq. (13) suggests that the plasma has a complex conductivity $\sigma_c$ given by

$$\sigma_c \equiv \frac{\epsilon_0\omega_p^2}{-i\omega + \omega_c} \tag{14}$$

For the avoidance of complex conductivities, the plasma is considered to be a lossy dielectric. In this case the constitutive parameters are real, and they are found by substituting Eq. (13) for $\mathbf{j}(\mathbf{r}, t)$ into Maxwell's equations. If the resulting equations are cast into the standard form for a lossy dielectric, it follows that the conductivity of the plasma is given by

$$\sigma \equiv \frac{\epsilon_0\omega_c\omega_p^2}{\omega^2 + \omega_c^2}, \tag{15}$$

its permittivity is given by

$$\epsilon \equiv \epsilon_0\left(1 - \frac{\omega_p^2}{\omega^2 + \omega_c^2}\right) \tag{16}$$

and its permeability is given by

$$\mu \equiv \mu_0 \tag{17}$$

### B. Propagation Constant of a Plasma

Let a plasma be characterized by its electron concentration $n(\mathbf{r}, t)$, its collision frequency $f_c(\mathbf{r}, t)$, and its permeability $\mu = \mu_0$.

If $n(\mathbf{r}, t)$ and $f_c(\mathbf{r}, t)$ are slowly varying functions of position in the interior of the plasma, then the field quantities are continuous and have continuous derivatives and, therefore, satisfy Maxwell's equations.

Let $\mathbf{E}(\mathbf{r})$ and $\mathbf{H}(\mathbf{r})$ be the complex electric and magnetic field vectors in the plasma defined respectively by

$$\mathbf{E}(\mathbf{r}) \equiv \mathrm{Re}\{\mathscr{E}(\mathbf{r}, t)\, e^{-i\omega t}\} \tag{18}$$

$$\mathbf{H}(\mathbf{r}) \equiv \mathrm{Re}\{\mathscr{H}(\mathbf{r}, t)\, e^{-i\omega t}\} \tag{19}$$

where $\mathscr{E}(\mathbf{r}, t)$ and $\mathscr{H}(\mathbf{r}, t)$ are the real electric and magnetic field vectors in the plasma, respectively. For a linear, isotropic, and homogeneous plasma,

$$\mathbf{D}(\mathbf{r}) = \epsilon\mathbf{E}(\mathbf{r}) \tag{20}$$

$$\mathbf{B}(\mathbf{r}) = \mu_0\mathbf{H}(\mathbf{r}) \tag{21}$$

$$\mathbf{j}(\mathbf{r}) = \sigma\mathbf{E}(\mathbf{r}) \tag{22}$$

where the complex vectors $\mathbf{D}(\mathbf{r})$, $\mathbf{B}(\mathbf{r})$, and $\mathbf{j}(\mathbf{r})$ represent the electric flux density, the magnetic flux density, and the electric current density of the plasma, respectively, and $\epsilon$, $\mu$, and $\sigma$ are the constitutive parameters of the plasma as found in the previous section.

With $e^{-i\omega t}$ time-dependence, Maxwell's two independent equations take the following steady state form in the plasma:

$$\nabla \wedge \mathbf{E}(\mathbf{r}) = i\omega\mu_0\mathbf{H}(\mathbf{r}) \tag{23}$$

$$\nabla \wedge \mathbf{H}(\mathbf{r}) = (\sigma - i\omega\epsilon)\mathbf{E}(\mathbf{r}) \tag{24}$$

If Eq. (24) is substituted into the curl of Eq. (23) and the resulting curl-curl operation is expanded, the wave equation for $\mathbf{E}(\mathbf{r})$ can be written in the form

$$(\nabla^2 + \gamma^2)\mathbf{E}(\mathbf{r}) = 0 \tag{25}$$

where the propagation constant $\gamma$ is given by

$$\gamma^2 \equiv \omega^2\mu_0\left(\epsilon + i\frac{\sigma}{\omega}\right) \tag{26}$$

The constant $\gamma$ is complex and, accordingly, is written in the form

$$\gamma \equiv \beta + i\alpha \qquad (\beta, \alpha = \text{positive-definite}) \tag{27}$$

which displays the phase factor $\beta$ and the attenuation factor $\alpha$. Explicit expressions for $\beta$ and $\alpha$ in terms of the constitutive parameters are found by substituting Eq. (27)

into Eq. (26). It follows that

$$\beta = \omega \sqrt{\frac{\mu_0}{2}} \sqrt{\left[\epsilon + \sqrt{\left(\epsilon^2 + \frac{\sigma^2}{\omega^2}\right)}\right]} \tag{28}$$

and

$$\alpha = \omega \sqrt{\frac{\mu_0}{2}} \sqrt{\left[-\epsilon + \sqrt{\left(\epsilon^2 + \frac{\sigma^2}{\omega^2}\right)}\right]} \tag{29}$$

To simplify the following discussion, it is assumed that the plasma is lossless. Since the losses are small (Ref. 3), this assumption is reasonable and introduces negligible error. For a lossless plasma with $\sigma = 0$, the expressions for $\beta$ and $\alpha$ become

$$\beta = \omega \sqrt{\left[\frac{\mu_0}{2}(\epsilon + |\epsilon|)\right]} \tag{30}$$

$$\alpha = \omega \sqrt{\left[\frac{\mu_0}{2}(-\epsilon + |\epsilon|)\right]} \tag{31}$$

Since $\epsilon = \epsilon_0 (1 - \omega_p^2/\omega^2)$ for a lossless plasma,

$$\beta = \frac{\omega}{c} \sqrt{\left(1 - \frac{\omega_p^2}{\omega^2}\right)} \qquad \alpha = 0 \qquad \text{for } \omega_p < \omega \tag{32}$$

and

$$\beta = 0 \qquad \alpha = \frac{\omega}{c} \sqrt{\left(\frac{\omega_p^2}{\omega^2} - 1\right)} \qquad \text{for } \omega_p > \omega \tag{33}$$

where the speed of light c in vacuum is defined by

$$c = \frac{1}{\sqrt{(\mu_0 \epsilon_0)}} \tag{34}$$

Therefore, if $\omega_p < \omega$, the wave travels without attenuation, and the plasma is said to be *underdense*. However, if $\omega_p > \omega$, the wave is evanescent and carries no power, and the plasma is said to be *overdense*. At $\omega_p = \omega$, the properties of the plasma change from underdense to overdense, and the wave is cut off. This frequency is called the critical radian plasma frequency $\omega_{pc}$.

Since the radian plasma frequency and the electron concentration are related by Eq. (12), a critical electron concentration $n_c$ can be found that corresponds to each

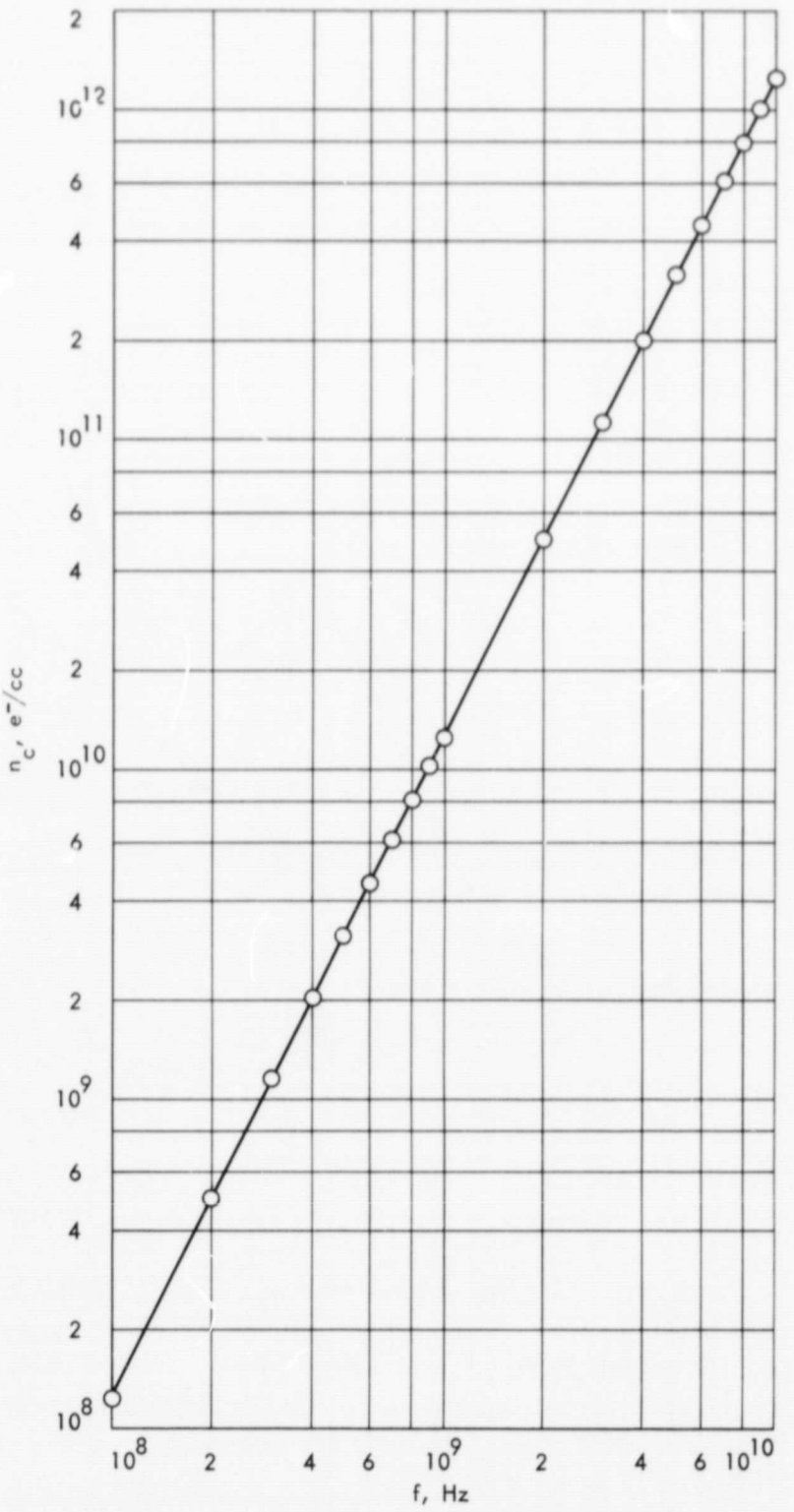


**Fig. 6. Critical electron concentration vs frequency**

critical radian plasma frequency $\omega_{pc}$. The critical electron concentration $n_c$ in terms of the signal frequency $f$ is therefore

$$n_c = \frac{4\pi^2 f^2 m \epsilon_0}{q^2} \tag{35}$$

Loss of the transmitted signal will occur if the electron concentration exceeds the critical electron concentration during entry into the Martian atmosphere.

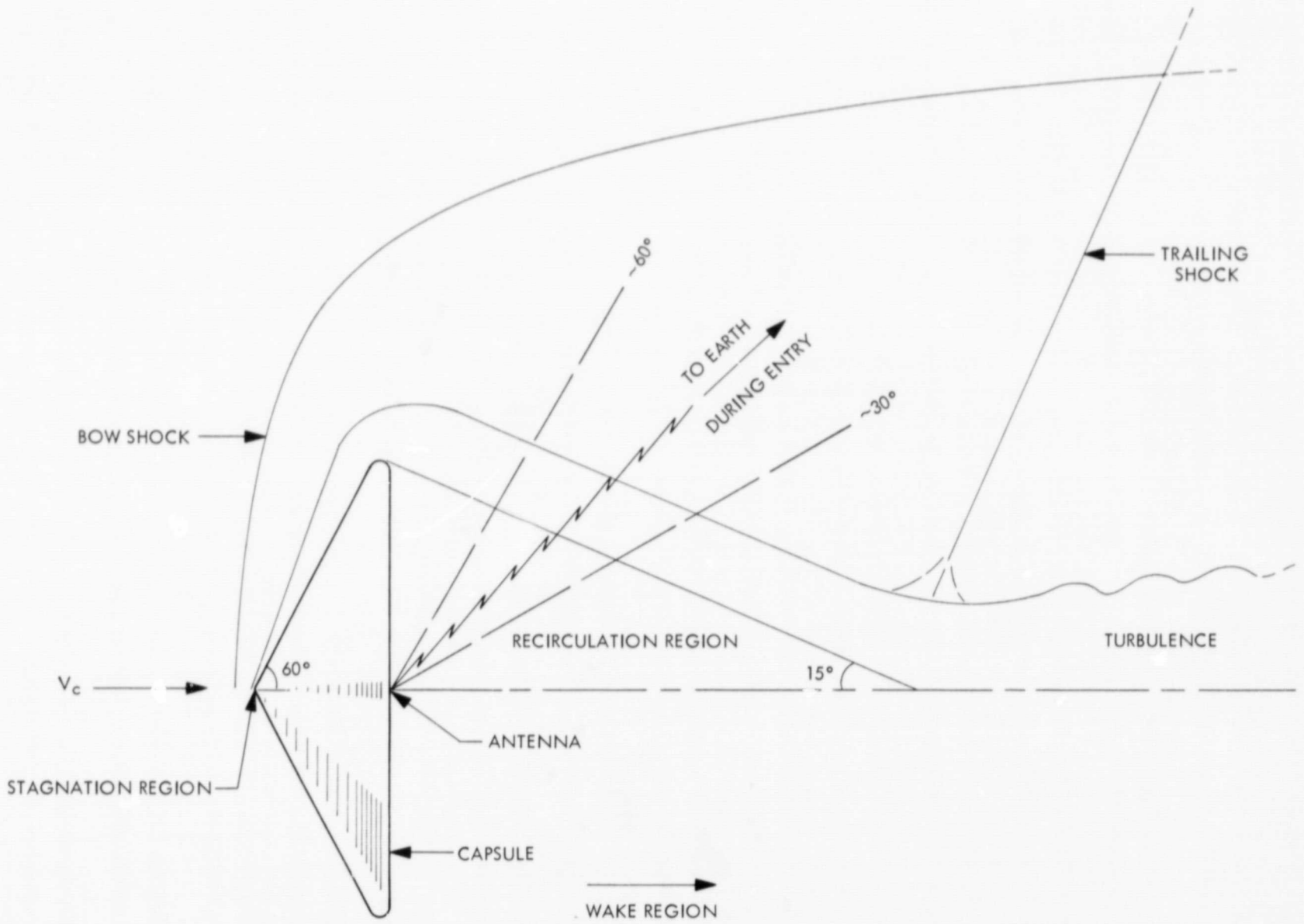


**Fig. 7. Plasma environment model**

From Eq. (35), the critical electron concentration for 400 MHz is $1.99 \times 10^9$ $e^-$/cc, and the critical electron concentration for 2.295 GHz is $6.53 \times 10^{10}$ $e^-$/cc. The values of the critical electron concentration for frequencies other than 400 MHz and 2.295 GHz are shown graphically in Fig. 6.

### C. Electron Concentration

#### *1. Stagnation region*

An exact analysis of the electron concentration in the stagnation region (Fig. 7) of the capsule during entry into the Martian atmosphere is not attempted here because the analysis would require the use of nonequilibrium chemistry to obtain the solution. Instead, this analysis uses an approximate solution based on chemical equilibrium in the stagnation region and is applicable only in the dense region of the atmosphere where the chemical reaction rates are sufficiently fast for the assumption of chemical equilibrium to be reasonable (Ref. 3). However, an equilibrium solution at less dense altitudes would produce a conservative estimate of the electron concentration and, therefore, will be in keeping with the objective of this study.

With the use of an equilibrium thermochemistry and normal-shock computer program (Ref. 7), the equilibrium electron concentration behind a traveling normal shock is determined. This is a close approximation to the actual electron concentration in the stagnation region of a blunt entry capsule.

The input parameters to the program are

initial mixture constituents
initial mole fraction compositions
initial molal enthalpies
initial free stream temperature
initial free stream pressure
shock temperature.

The output of the program is a complete thermodynamic and chemical description of the gases behind the normal shock.

The output parameters of interest to this report are the shock velocity and electron concentration behind the normal shock. Since it is convenient to plot the output parameters against altitude and since the program input is expressed in terms of initial free stream pressure, Eqs. (1) and (3) are used to convert each altitude of interest into an equivalent initial free stream pressure.

Since the input value of the shock temperature cannot be determined in advance, the electron concentration in the stagnation region of the capsule is calculated for a series of shock temperatures. The program output then gives the appropriate electron concentration and shock velocity corresponding to each shock temperature in the series, from which a curve of electron concentration vs shock velocity is developed for each initial free stream pressure, with the shock temperature as a parameter along the curve. The correct shock velocity for each curve is the velocity of the capsule for that curve; and the capsule velocity corresponding to the free stream pressure along each curve is given by Eq. (7). Equation (7) can, in turn, be used for the determination of the electron concentration in the stagnation region of the entry capsule as a function of capsule velocity by linear interpolation, when necessary.

Figure 8 shows graphs of the electron concentration in the stagnation region of the capsule vs shock velocity or capsule velocity. These graphs were obtained for the VM-4 and VM-8 model atmospheres by the method just described from the thermochemistry and normal-shock computer program. The curves used to construct these graphs are also shown.

### 2. *Wake region*

The electron concentration in the wake region (Fig. 7) is calculated since the antenna will be mounted on the rear part of the capsule and the propagation path will be through the wake region (Ref. 1).

Again, no exact analysis is attempted and a frozen flow approximation to the actual flow conditions is used to estimate the value of the electron concentration in the wake region of the capsule (Ref. 3). It is assumed that the total number of electrons formed in the stagnation region remains constant as the gases flow around the capsule and into the wake region. Any change in the electron concentration is due to the expansion of the gases as they flow into the wake region. The value of the specific heat ratio is not a constant during the expansion of the gases; however, the results are not sensitive to the value selected (Ref. 3).

The value of the electron concentration $n_w$ in the wake region is related to the value of the electron concentration $n_s$ in the stagnation region by (Ref. 5)

$$n_w = n_s \left( \frac{p_\infty}{p_s} \right)^{1/\gamma} \tag{36}$$

where the pressure ratio $p_s/p_\infty$ across the shock is obtained from the output of the thermochemistry and normal-shock computer program, and $\gamma$ is the specific heat ratio.

Graphs of electron concentration in the wake region vs altitude, and electron concentration in the wake region vs time-from-entry, can be obtained from Fig. 8 by using Eq. (36) and the relationships between capsule velocity, altitude, and capsule time-from-entry as given by Eqs. (7) and (8). These graphs are shown in Figs. 9 and 10 for the VM-4 and VM-8 model atmospheres. Note that the values of the electron concentration between 22 km and 100 km for the VM-4 model atmosphere and between 20 km and 80 km for the VM-8 model atmosphere were obtained from the thermochemistry and normal-shock computer program.

## V. Conclusion

As is evident from an examination of the graphs of electron concentration in the wake region vs capsule altitude or time-from-entry, blackout will occur during entry of a blunt capsule into the Martian atmosphere.

The electron concentration in the wake region reaches a peak of $7.7 \times 11$ $e^-$/cc at an altitude of 29 km for the VM-4 model atmosphere and reaches a peak of $7.9 \times 10^{10}$ $e^-$/cc at an altitude of 29 km for the VM-8 model atmosphere.

In the VM-4 model atmosphere, blackout begins at an altitude of 66 km and ends at an altitude of 22 km for the 400-MHz signal, and begins at an altitude of 47 km and ends at an altitude of 24 km for the 2.295-GHz signal. The duration of blackout is 8.5 s for the 400-MHz signal and 4.5 s for the 2.295-GHz signal. Similarly, in the VM-8 model atmosphere, blackout begins at an altitude of 53 km and ends at an altitude of 23 km for the 400-MHz signal, and begins at an altitude of 33 km and ends at an altitude of 27 km for the 2.295-GHz signal. The duration

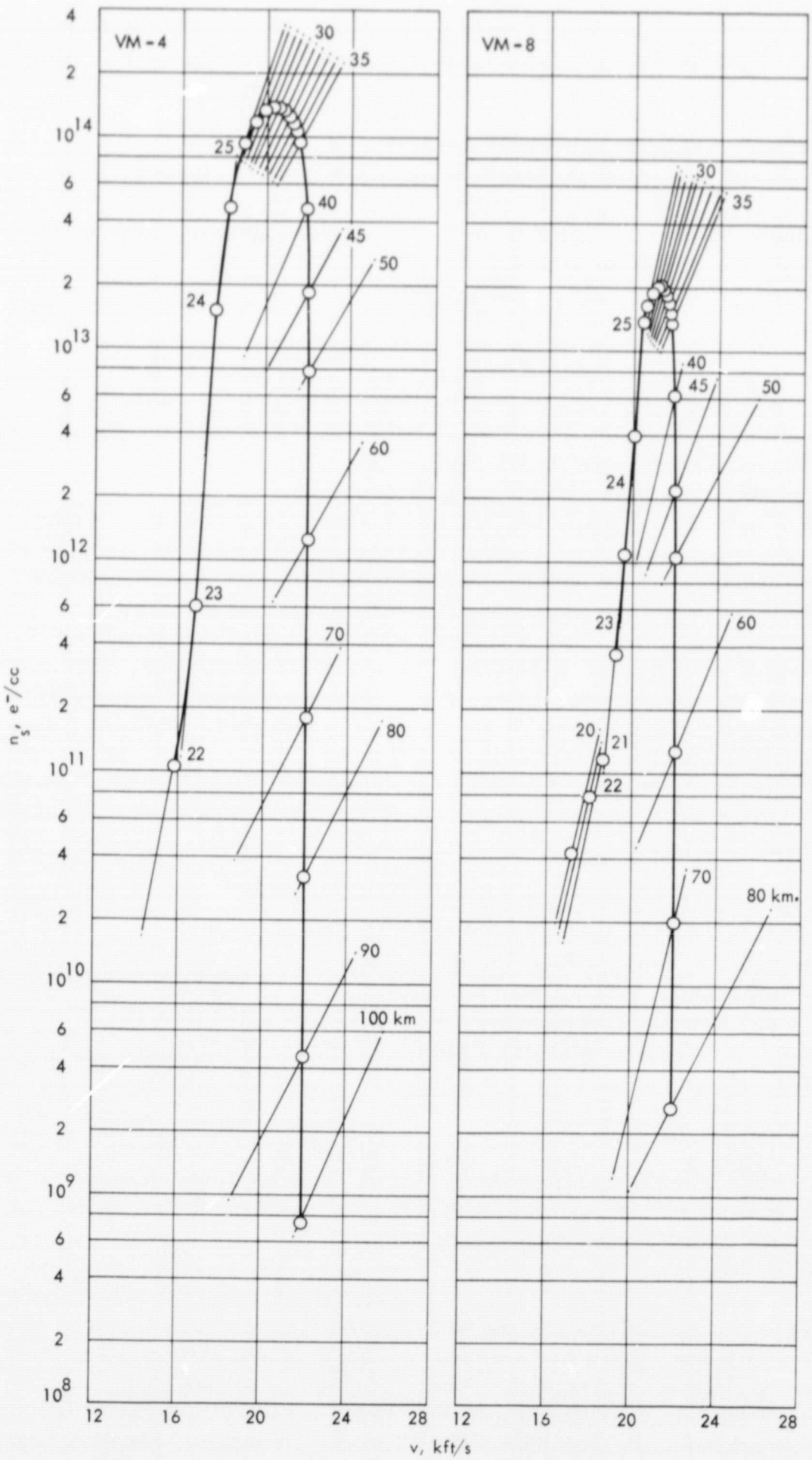


**Fig. 8. Electron concentration in stagnation region vs capsule velocity for two model atmospheres**

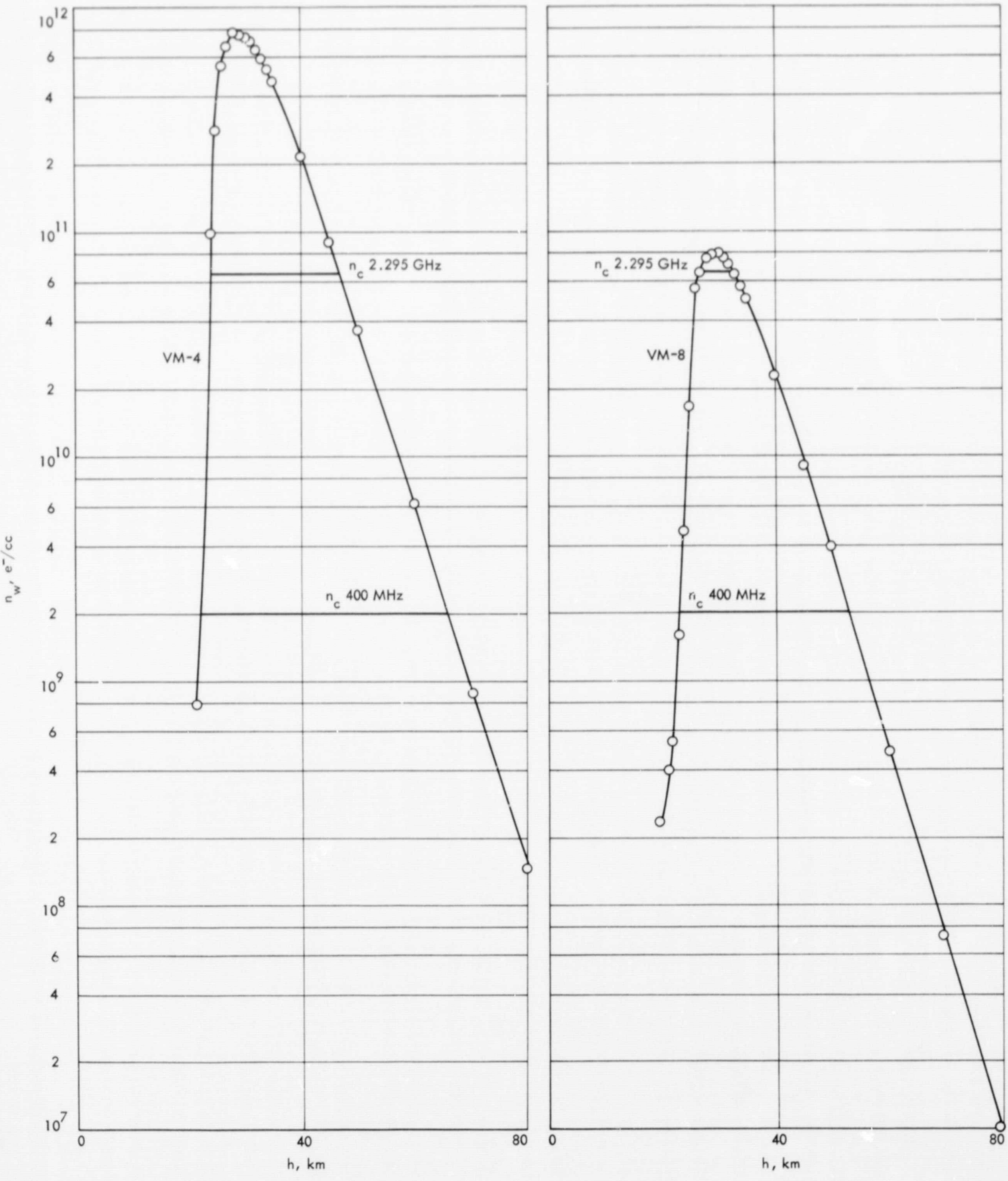


**Fig. 9. Electron concentration in wake region vs capsule altitude for two model atmospheres**

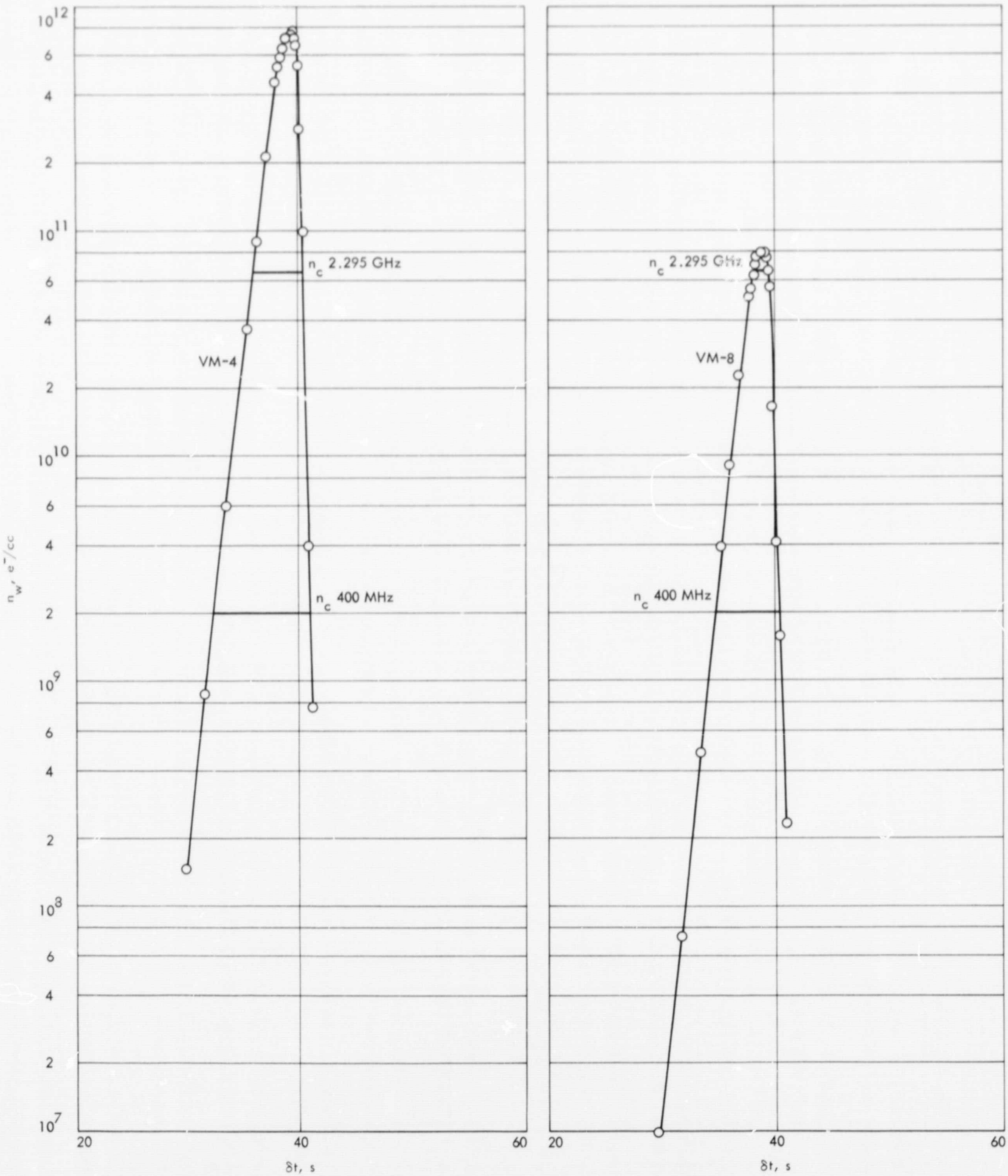


**Fig. 10. Electron concentration in wake region vs capsule time-from-entry for two model atmospheres**

of blackout is 5.7 s for the 400-MHz signal and 1.3 s for the 2.295-GHz signal.

Blackout can be reduced or eliminated by entering the atmosphere at lower velocities, by transmitting at higher frequencies, or by injecting high-electron-affinity fluids into the wake region. The latter alternative has been examined by D. F. Spencer (Ref. 3) and the feasibility of the first and second alternatives will be the subjects of future investigations.

# Appendix
# The Calculation of Linear Entry-Trajectories: A Computer Program

## I. Program Description

The purpose of this program, which has been specifically developed for use with the Martian entry propagation study, is to determine the linear entry-trajectory characteristics of a blunt capsule as it descends through a Mars-type planetary atmosphere subject to arbitrary initial entry conditions. Actually, the development of the program is such that any hypothetical planetary atmosphere can be used in the calculations of the entry-trajectory characteristics of the capsule. The characteristics of interest to this study are the velocity and elapsed time-from-entry of the capsule as a function of attitude. The source language is FORTRAN II for use on an IBM 1620 computer or equivalent.

### A. Input Requirements

To compute the entry-trajectory characteristics, the pressure and density profiles of the atmosphere must first be developed. This program develops these profiles from the assumed physical properties of the atmosphere. The required input data to the program are

(1) Atmospheric properties
- surface pressure
- surface density
- surface temperature
- specific heat ratio
- adiabatic lapse rate
- tropopause attitude
- inverse scale height

(2) Entry parameters
- entry attitude
- entry velocity
- entry angle
- ballistic coefficient

### B. Output

The output of the program includes the pressure and density profiles of the atmosphere and the velocity and time-from-entry of the capsule. The various outputs of the program are calculated at points from the surface of the planet to any arbitrary altitude above the surface to the planet in arbitrary increments in altitude.

### C. Program Limitations

Although the program has certain limitations, they are entirely in keeping with the study.

The limitations follow.

(1) The trajectory is assumed to be a straight path at the constant entry angle relative to the local horizontal at the assumed point of entry into the atmosphere.

(2) The surface of the planet is assumed to be flat so that the altitude of the capsule above the surface of the planet is independent of the displacement of the capsule from the assumed point of entry into the atmosphere.

(3) Above the tropopause altitude, the planetary atmosphere is assumed to be isothermal at the stratospheric temperature so that the pressure and density profiles obey simple exponential decay laws.

## II. Calculations

### A. Atmospheric Characteristics

The pressure and density profiles of the atmosphere are given respectively by

$$p = \begin{cases} p_0 \left(1 + \dfrac{\Gamma}{T_0} h\right)^{\gamma/(\gamma-1)} & 0 \leq h \leq h_t \\ p_t \, e^{-\beta(h-h_t)} & h > h_t \end{cases}$$

and by

$$\rho = \begin{cases} \rho_0 \left(1 + \dfrac{\Gamma}{T_0} h\right)^{1/(\gamma-1)} & 0 \leq h \leq h_t \\ \rho_t \, e^{-\beta(h-h_t)} & h > h_t \end{cases}$$

where $p_0$ is the surface pressure, $\rho_0$ is the surface density, $T_0$ is the surface temperature, $\gamma$ is the specific heat ratio, $\Gamma$ is the adiabatic lapse rate, $h_t$ is the tropopause altitude, $p_t$ is the pressure of the tropopause altitude, and $\rho_t$ is the density at the tropopause altitude.

### B. Entry-Trajectory Characteristics

The velocity $v$ and time-from-entry $\delta t$ of the capsule are given respectively by

$$v = v_e\, e^{-p/2g_s\Delta \sin\psi_e}$$

and

$$\delta t = \frac{1}{\beta v_e \sin\psi_e}\left[ Ei\left(\frac{p}{2g_s\Delta \sin\psi_e}\right) - Ei\left(\frac{p_e}{2g_s\Delta \sin\psi_e}\right)\right]$$

where

$$Ei(\zeta) \equiv \int_{-\infty}^{\zeta} d\eta \frac{e^{\eta}}{\eta} \qquad \text{for } \zeta > 0$$

In these equations, $p_e$ is the pressure at the entry altitude, $v_e$ is the entry velocity, $\psi_e$ is the entry angle, $\Delta$ is the ballistic coefficient, $g_s$ is the surface gravity, $\beta$ is the inverse scale height, and $Ei(\zeta)$ is the exponential integral function.

## III. Usage

### A. Definitions

Program usage is given in the form of tables that follow. Input and output data are shown in Tables A-1, A-2, and A-3.

**Table A-1. Input definitions**

| Program name | Symbol | Property | Unit |
|---|---|---|---|
| PO | $p_0$ | Surface pressure | mbar |
| DO | $\rho_0$ | Surface density | $10^{-5}$g/cc |
| TO | $T_0$ | Surface temperature | °K |
| SG | $g_s$ | Surface gravity | cm/s$^2$ |
| SHR | $\gamma$ | Specific heat ratio | — |
| ALR | $\Gamma$ | Adiabatic lapse rate | °K/km |
| HT | $h_t$ | Tropopause altitude | km |
| SHI | $\beta$ | Inverse scale height | km$^{-1}$ |
| HE | $h_e$ | Entry altitude | kft |
| VE | $v_e$ | Entry velocity | kft/s |
| EA | $\psi_e$ | Entry angle | deg |
| BC | $\Delta$ | Ballistic coefficient | slugs/ft$^2$ |
| ALT | $a$ | Altitude to which calculations extend | km |
| DELTA | $\delta$ | Increment in altitude between calculations | km |

**Table A-2. Input data**

| Card number | Program name | Format |
|---|---|---|
| 1 | PO, DO, TO, SG, SHR, ALR, HT, SHI | 8F10.0 |
| 2 | HE, VE, EA, BC, ALT, DELTA | 6F10.0 |

**Table A-3. Output definitions**

| Program name | Symbol | Property | Unit |
|---|---|---|---|
| H | $h$ | Altitude | km |
| HC | $h_c$ | Altitude | kft |
| P | $p$ | Pressure | mbar |
| PC | $p_c$ | Pressure | p/ft$^2$ |
| PA | $p_a$ | Pressure | atm |
| D | $\rho$ | Density | $10^{-5}$g/cc |
| DC | $\rho_c$ | Density | $10^{-5}$ slugs/ft$^3$ |
| V | $v$ | Velocity | km/s |
| VC | $v_c$ | Velocity | kft/s |
| T | $T$ | Time-from-entry | s |

## B. Sample Output Data

### *1. The VM-4 model atmosphere.*

```
SURFACE PRESSURE       =    10.000 (MB)
SURFACE DENSITY        =     2.570 (E-05 G/CC)
SURFACE TEMPERATURE    =   200.000 (DEG.K)
SURFACE GRAVITY        =   375.000 (CM/SQ.S)
SPECIFIC HEAT RATIO    =     1.430
ADIABATIC LAPSE RATE   =    -5.850 (DEG.K/KM)
TROPOPAUSE ALTITUDE    =    17.100 (KM)
INVERSE SCALE HEIGHT   =      .193 (1/KM)

ENTRY ALTITUDE         =   800.000 (KF)
ENTRY VELOCITY         =    22.000 (KF/S)
ENTRY ANGLE            =    55.000 (DEGREES)
BALLISTIC COEFFICIENT  =      .120 (SLUGS/SQ.F)
```

| ALTITUDE (KM) | ALTITUDE (KF) | PRESSURE (MB) | PRESSURE (P/SQ.F) | PRESSURE (ATMSPHRS) | DENSITY (E-05 G/CC) | DENSITY (E-05 SLUGS/CU.F) |
|---|---|---|---|---|---|---|
| 0.000 | 0.000 | 1.0000000E+01 | 2.0885514E+01 | 9.8692000E-03 | 2.5700000E+00 | 4.9866308E+00 |
| 1.000 | 3.280 | 9.0599252E+00 | 1.8922119E+01 | 8.9414213E-03 | 2.3985585E+00 | 4.6539789E+00 |
| 2.000 | 6.561 | 8.1834675E+00 | 1.7091592E+01 | 8.0764277E-03 | 2.2338302E+00 | 4.3343527E+00 |
| 3.000 | 9.842 | 7.3680988E+00 | 1.5388653E+01 | 7.2717240E-03 | 2.0757483E+00 | 4.0276227E+00 |
| 4.000 | 13.123 | 6.6113163E+00 | 1.3808073E+01 | 6.5248402E-03 | 1.9242449E+00 | 3.7336572E+00 |
| 5.000 | 16.404 | 5.9106429E+00 | 1.2344631E+01 | 5.8333316E-03 | 1.7792506E+00 | 3.4523213E+00 |
| 6.000 | 19.684 | 5.2636285E+00 | 1.0993358E+01 | 5.1947802E-03 | 1.6406943E+00 | 3.1834773E+00 |
| 7.000 | 22.965 | 4.6678501E+00 | 9.7490448E+00 | 4.6067946E-03 | 1.5085035E+00 | 2.9269844E+00 |
| 8.000 | 26.246 | 4.1209123E+00 | 8.6067371E+00 | 4.0670107E-03 | 1.3826037E+00 | 2.6826981E+00 |
| 9.000 | 29.527 | 3.6204484E+00 | 7.5614925E+00 | 3.5730929E-03 | 1.2629185E+00 | 2.4504701E+00 |
| 10.000 | 32.808 | 3.1641213E+00 | 6.6084299E+00 | 3.1227345E-03 | 1.1493697E+00 | 2.2301488E+00 |
| 11.000 | 36.089 | 2.7496226E+00 | 5.7427281E+00 | 2.7136575E-03 | 1.0418768E+00 | 2.0215778E+00 |
| 12.000 | 39.369 | 2.3746766E+00 | 4.9596341E+00 | 2.3436158E-03 | 9.4035734E-01 | 1.8245972E+00 |
| 13.000 | 42.650 | 2.0370384E+00 | 4.2544594E+00 | 2.0103939E-03 | 8.4472587E-01 | 1.6390412E+00 |
| 14.000 | 45.931 | 1.7344956E+00 | 3.6225832E+00 | 1.7118083E-03 | 7.5489476E-01 | 1.4647398E+00 |
| 15.000 | 49.212 | 1.4648699E+00 | 3.0594560E+00 | 1.4457094E-03 | 6.7077344E-01 | 1.3015173E+00 |
| 16.000 | 52.493 | 1.2260180E+00 | 2.5606016E+00 | 1.2099816E-03 | 5.9226814E-01 | 1.1491916E+00 |
| 17.000 | 55.774 | 1.0158325E+00 | 2.1216183E+00 | 1.0025454E-03 | 5.1928181E-01 | 1.0075745E+00 |
| 18.000 | 59.054 | 8.3744778E-01 | 1.7490527E+00 | 8.2649396E-04 | 4.3059889E-01 | 8.3550105E-01 |
| 19.000 | 62.335 | 6.9046060E-01 | 1.4420624E+00 | 6.8142937E-04 | 3.5502102E-01 | 6.8885555E-01 |
| 20.000 | 65.616 | 5.6927231E-01 | 1.1889544E+00 | 5.6182622E-04 | 2.9270843E-01 | 5.6794898E-01 |
| 21.000 | 68.897 | 4.6935474E-01 | 9.8027149E-01 | 4.6321558E-04 | 2.4133282E-01 | 4.6826369E-01 |
| 22.000 | 72.178 | 3.8697454E-01 | 8.0821621E-01 | 3.8191291E-04 | 1.9897456E-01 | 3.8607497E-01 |
| 23.000 | 75.459 | 3.1905353E-01 | 6.6635969E-01 | 3.1488030E-04 | 1.6405094E-01 | 3.1831186E-01 |
| 24.000 | 78.739 | 2.6305389E-01 | 5.4940157E-01 | 2.5961314E-04 | 1.3525704E-01 | 2.6244238E-01 |
| 25.000 | 82.020 | 2.1688319E-01 | 4.5297169E-01 | 2.1404635E-04 | 1.1151699E-01 | 2.1637901E-01 |
| 26.000 | 85.301 | 1.7881628E-01 | 3.7346699E-01 | 1.7647736E-04 | 9.1943753E-02 | 1.7840060E-01 |
| 27.000 | 88.582 | 1.4743080E-01 | 3.0791680E-01 | 1.4550240E-04 | 7.5805968E-02 | 1.4708808E-01 |
| 28.000 | 91.863 | 1.2155403E-01 | 2.5387183E-01 | 1.1996410E-04 | 6.2500653E-02 | 1.2127147E-01 |
| 29.000 | 95.144 | 1.0021911E-01 | 2.0931276E-01 | 9.8908244E-05 | 5.1530662E-02 | 9.9986144E-02 |
| 30.000 | 98.424 | 8.2628850E-02 | 1.7257460E-01 | 8.1548064E-05 | 4.2486101E-02 | 8.2436771E-02 |
| 31.000 | 101.705 | 6.8125997E-02 | 1.4228464E-01 | 6.7234908E-05 | 3.5029024E-02 | 6.7967631E-02 |
| 32.000 | 104.986 | 5.6168657E-02 | 1.1731112E-01 | 5.5433970E-05 | 2.8880799E-02 | 5.6038087E-02 |
| 33.000 | 108.267 | 4.6310045E-02 | 9.6720909E-02 | 4.5704309E-05 | 2.3811698E-02 | 4.6202392E-02 |
| 34.000 | 111.548 | 3.8181796E-02 | 7.9744643E-02 | 3.7682378E-05 | 1.9632315E-02 | 3.8093038E-02 |
| 35.000 | 114.829 | 3.1480203E-02 | 6.5748022E-02 | 3.1068441E-05 | 1.6186490E-02 | 3.1407023E-02 |
| 36.000 | 118.109 | 2.5954861E-02 | 5.4208061E-02 | 2.5615371E-05 | 1.3345470E-02 | 2.5894526E-02 |
| 37.000 | 121.390 | 2.1399314E-02 | 4.4693567E-02 | 2.1119410E-05 | 1.1003099E-02 | 2.1349569E-02 |
| 38.000 | 124.671 | 1.7643349E-02 | 3.6849041E-02 | 1.7412573E-05 | 9.0718572E-03 | 1.7602335E-02 |
| 39.000 | 127.952 | 1.4546623E-02 | 3.0381369E-02 | 1.4356353E-05 | 7.4795827E-03 | 1.4512808E-02 |
| 40.000 | 131.233 | 1.1993428E-02 | 2.5048890E-02 | 1.1836553E-05 | 6.1667812E-03 | 1.1965549E-02 |
| 41.000 | 134.514 | 9.8883659E-03 | 2.0652360E-02 | 9.7590260E-06 | 5.0843999E-03 | 9.8653795E-03 |
| 42.000 | 137.794 | 8.1527794E-03 | 1.7027498E-02 | 8.0461410E-06 | 4.1919960E-03 | 8.1338275E-03 |
| 43.000 | 141.075 | 6.7218196E-03 | 1.4038865E-02 | 6.6338981E-06 | 3.4562251E-03 | 6.7061940E-03 |
| 44.000 | 144.356 | 5.5420191E-03 | 1.1574791E-02 | 5.4695294E-06 | 2.8495953E-03 | 5.5291361E-03 |
| 45.000 | 147.637 | 4.5692949E-03 | 9.5432072E-03 | 4.5095285E-06 | 2.3494400E-03 | 4.5586731E-03 |
| 46.000 | 150.918 | 3.7673012E-03 | 7.8682021E-03 | 3.7180249E-06 | 1.9370709E-03 | 3.7585438E-03 |
| 47.000 | 154.199 | 3.1060718E-03 | 6.4871906E-03 | 3.0654443E-06 | 1.5970799E-03 | 3.0988513E-03 |
| 48.000 | 157.479 | 2.5609003E-03 | 5.3485719E-03 | 2.5274037E-06 | 1.3167637E-03 | 2.5549472E-03 |
| 49.000 | 160.760 | 2.1114162E-03 | 4.4098012E-03 | 2.0837988E-06 | 1.0856479E-03 | 2.1065079E-03 |
| 50.000 | 164.041 | 1.7408245E-03 | 3.6358014E-03 | 1.7180545E-06 | 8.9509718E-04 | 1.7367779E-03 |

| ALTITUDE (KM) | ALTITUDE (KF) | VELOCITY (KM/S) | VELOCITY (KF/S) | TIME FROM ENTRY (SEC.) |
|---|---|---|---|---|
| 0.000 | 0.000 | 1.1922950E-03 | 3.9117211E-03 | 7.5498175E+02 |
| 1.000 | 3.280 | 2.6848309E-03 | 8.8084826E-03 | 3.9866235E+02 |
| 2.000 | 6.561 | 5.7226001E-03 | 1.8774896E-02 | 2.3159600E+02 |
| 3.000 | 9.842 | 1.1570739E-02 | 3.7961665E-02 | 1.4882312E+02 |
| 4.000 | 13.123 | 2.2241225E-02 | 7.2969751E-02 | 1.0558084E+02 |
| 5.000 | 16.404 | 4.0730062E-02 | 1.3362854E-01 | 8.1810625E+01 |
| 6.000 | 19.684 | 7.1211314E-02 | 2.3363245E-01 | 6.8090523E+01 |
| 7.000 | 22.965 | 1.1911574E-01 | 3.9079888E-01 | 5.9792145E+01 |
| 8.000 | 26.246 | 1.9101780E-01 | 6.2669755E-01 | 5.4543295E+01 |
| 9.000 | 29.527 | 2.9427307E-01 | 9.6546088E-01 | 5.1078228E+01 |
| 10.000 | 32.808 | 4.3639092E-01 | 1.4317258E+00 | 4.8695389E+01 |
| 11.000 | 36.089 | 6.2418741E-01 | 2.0478548E+00 | 4.6991715E+01 |
| 12.000 | 39.369 | 8.6282314E-01 | 2.8307788E+00 | 4.5727615E+01 |
| 13.000 | 42.650 | 1.1548829E+00 | 3.7889782E+00 | 4.4756002E+01 |
| 14.000 | 45.931 | 1.4996612E+00 | 4.9201384E+00 | 4.3983745E+01 |
| 15.000 | 49.212 | 1.8927980E+00 | 6.2099547E+00 | 4.3350099E+01 |
| 16.000 | 52.493 | 2.3263498E+00 | 7.6323658E+00 | 4.2814256E+01 |
| 17.000 | 55.774 | 2.7893033E+00 | 9.1512391E+00 | 4.2347964E+01 |
| 18.000 | 59.054 | 3.2538011E+00 | 1.0675179E+01 | 4.1943126E+01 |
| 19.000 | 62.335 | 3.6941285E+00 | 1.2119819E+01 | 4.1591493E+01 |
| 20.000 | 65.616 | 4.1016469E+00 | 1.3456819E+01 | 4.1278259E+01 |
| 21.000 | 68.897 | 4.4712392E+00 | 1.4669390E+01 | 4.0993502E+01 |
| 22.000 | 72.178 | 4.8008809E+00 | 1.5750889E+01 | 4.0730260E+01 |
| 23.000 | 75.459 | 5.0908662E+00 | 1.6702283E+01 | 4.0483525E+01 |
| 24.000 | 78.739 | 5.3430822E+00 | 1.7529762E+01 | 4.0249614E+01 |
| 25.000 | 82.020 | 5.5604011E+00 | 1.8242749E+01 | 4.0025775E+01 |
| 26.000 | 85.301 | 5.7462091E+00 | 1.8852354E+01 | 3.9809910E+01 |
| 27.000 | 88.582 | 5.9040652E+00 | 1.9370253E+01 | 3.9600405E+01 |
| 28.000 | 91.863 | 6.0374713E+00 | 1.9807936E+01 | 3.9396003E+01 |
| 29.000 | 95.144 | 6.1497263E+00 | 2.0176226E+01 | 3.9195714E+01 |
| 30.000 | 98.424 | 6.2438467E+00 | 2.0485020E+01 | 3.8998753E+01 |
| 31.000 | 101.705 | 6.3225298E+00 | 2.0743166E+01 | 3.8804495E+01 |
| 32.000 | 104.986 | 6.3881478E+00 | 2.0958448E+01 | 3.8612437E+01 |
| 33.000 | 108.267 | 6.4427605E+00 | 2.1137623E+01 | 3.8422174E+01 |
| 34.000 | 111.548 | 6.4881386E+00 | 2.1286501E+01 | 3.8233378E+01 |
| 35.000 | 114.829 | 6.5257925E+00 | 2.1410037E+01 | 3.8045785E+01 |
| 36.000 | 118.109 | 6.5570016E+00 | 2.1512429E+01 | 3.7859175E+01 |
| 37.000 | 121.390 | 6.5828452E+00 | 2.1597217E+01 | 3.7673374E+01 |
| 38.000 | 124.671 | 6.6042294E+00 | 2.1667375E+01 | 3.7488236E+01 |
| 39.000 | 127.952 | 6.6219126E+00 | 2.1725391E+01 | 3.7303644E+01 |
| 40.000 | 131.233 | 6.6365276E+00 | 2.1773340E+01 | 3.7119499E+01 |
| 41.000 | 134.514 | 6.6486017E+00 | 2.1812953E+01 | 3.6935724E+01 |
| 42.000 | 137.794 | 6.6585731E+00 | 2.1845668E+01 | 3.6752252E+01 |
| 43.000 | 141.075 | 6.6668055E+00 | 2.1872677E+01 | 3.6569030E+01 |
| 44.000 | 144.356 | 6.6736007E+00 | 2.1894971E+01 | 3.6386014E+01 |
| 45.000 | 147.637 | 6.6792084E+00 | 2.1913369E+01 | 3.6203167E+01 |
| 46.000 | 150.918 | 6.6838354E+00 | 2.1928549E+01 | 3.6020460E+01 |
| 47.000 | 154.199 | 6.6876527E+00 | 2.1941073E+01 | 3.5837868E+01 |
| 48.000 | 157.479 | 6.6908017E+00 | 2.1951405E+01 | 3.5655371E+01 |
| 49.000 | 160.760 | 6.6933990E+00 | 2.1959926E+01 | 3.5472952E+01 |
| 50.000 | 164.041 | 6.6955412E+00 | 2.1966954E+01 | 3.5290597E+01 |

## 2. The VM-8 model atmosphere.

| | | |
|---|---|---|
| SURFACE PRESSURE | = | 5.000 (MB) |
| SURFACE DENSITY | = | 1.320 (E-05 G/CC) |
| SURFACE TEMPERATURE | = | 200.000 (DEG.K) |
| SURFACE GRAVITY | = | 375.000 (CM/SQ.S) |
| SPECIFIC HEAT RATIO | = | 1.370 |
| ADIABATIC LAPSE RATE | = | -5.390 (DEG.K/KM) |
| TROPOPAUSE ALTITUDE | = | 18.600 (KM) |
| INVERSE SCALE HEIGHT | = | .199 (1/KM) |
| ENTRY ALTITUDE | = | 800.000 (KF) |
| ENTRY VELOCITY | = | 22.000 (KF/S) |
| ENTRY ANGLE | = | 55.000 (DEGREES) |
| BALLISTIC COEFFICIENT | = | .120 (SLUGS/SQ.F) |

| ALTITUDE (KM) | ALTITUDE (KF) | PRESSURE (MB) | PRESSURE (P/SQ.F) | PRESSURE (ATMSPHRS) | DENSITY (E-05 G/CC) | DENSITY (E-05 SLUGS/CU.F) |
|---|---|---|---|---|---|---|
| 0.000 | 0.000 | 5.0000000E+00 | 1.0442757E+01 | 4.9346000E-03 | 1.3200000E+00 | 2.5612267E+00 |
| 1.000 | 3.280 | 4.5189550E+00 | 9.4380697E+00 | 4.4598470E-03 | 1.2260460E+00 | 2.3789256E+00 |
| 2.000 | 6.561 | 4.0726025E+00 | 8.5058396E+00 | 4.0193328E-03 | 1.1364201E+00 | 2.2050223E+00 |
| 3.000 | 9.842 | 3.6593226E+00 | 7.6426833E+00 | 3.6114586E-03 | 1.0510375E+00 | 2.0393525E+00 |
| 4.000 | 13.123 | 3.2775274E+00 | 6.8452844E+00 | 3.2346573E-03 | 9.6981309E-01 | 1.8817509E+00 |
| 5.000 | 16.404 | 2.9256615E+00 | 6.1103944E+00 | 2.8873938E-03 | 8.9266065E-01 | 1.7320502E+00 |
| 6.000 | 19.684 | 2.6022020E+00 | 5.4348326E+00 | 2.5681651E-03 | 8.1949342E-01 | 1.5900821E+00 |
| 7.000 | 22.965 | 2.3056592E+00 | 4.8154877E+00 | 2.2755011E-03 | 7.5022372E-01 | 1.4556765E+00 |
| 8.000 | 26.246 | 2.0345766E+00 | 4.2493178E+00 | 2.0079643E-03 | 6.8476314E-01 | 1.3286618E+00 |
| 9.000 | 29.527 | 1.7875313E+00 | 3.7333509E+00 | 1.7641503E-03 | 6.2302229E-01 | 1.2088646E+00 |
| 10.000 | 32.808 | 1.5631342E+00 | 3.2646861E+00 | 1.5426884E-03 | 5.6491088E-01 | 1.0961097E+00 |
| 11.000 | 36.089 | 1.3600307E+00 | 2.8404940E+00 | 1.3422414E-03 | 5.1033768E-01 | 9.9022009E-01 |
| 12.000 | 39.369 | 1.1769007E+00 | 2.4580176E+00 | 1.1615068E-03 | 4.5921044E-01 | 8.9101671E-01 |
| 13.000 | 42.650 | 1.0124595E+00 | 2.1145737E+00 | 9.9921652E-04 | 4.1143588E-01 | 7.9831862E-01 |
| 14.000 | 45.931 | 8.6545765E-01 | 1.8075527E+00 | 8.5413746E-04 | 3.6691958E-01 | 7.1194261E-01 |
| 15.000 | 49.212 | 7.3468140E-01 | 1.5344198E+00 | 7.2507176E-04 | 3.2556593E-01 | 6.3170315E-01 |
| 16.000 | 52.493 | 6.1895380E-01 | 1.2927168E+00 | 6.1085788E-04 | 2.8727814E-01 | 5.5741246E-01 |
| 17.000 | 55.774 | 5.1713430E-01 | 1.0800615E+00 | 5.1037018E-04 | 2.5195804E-01 | 4.8888005E-01 |
| 18.000 | 59.054 | 4.2812006E-01 | 8.9415075E-01 | 4.2252024E-04 | 2.1950611E-01 | 4.2591281E-01 |
| 19.000 | 62.335 | 3.5130627E-01 | 7.3372120E-01 | 3.4671118E-04 | 1.8596205E-01 | 3.6082649E-01 |
| 20.000 | 65.616 | 2.8791301E-01 | 6.0132112E-01 | 2.8414710E-04 | 1.5240518E-01 | 2.9571532E-01 |
| 21.000 | 68.897 | 2.3595907E-01 | 4.9281264E-01 | 2.3287272E-04 | 1.2490364E-01 | 2.4235344E-01 |
| 22.000 | 72.178 | 1.9338023E-01 | 4.0388455E-01 | 1.9085081E-04 | 1.0236477E-01 | 1.9862074E-01 |
| 23.000 | 75.459 | 1.5848475E-01 | 3.3100354E-01 | 1.5641176E-04 | 8.3893039E-02 | 1.6277961E-01 |
| 24.000 | 78.739 | 1.2988616E-01 | 2.7127392E-01 | 1.2818724E-04 | 6.8754532E-02 | 1.3340602E-01 |
| 25.000 | 82.020 | 1.0644819E-01 | 2.2232251E-01 | 1.0505584E-04 | 5.6347769E-02 | 1.0933288E-01 |
| 26.000 | 85.301 | 8.7239604E-02 | 1.8220439E-01 | 8.6098509E-05 | 4.6179808E-02 | 8.9603757E-02 |
| 27.000 | 88.582 | 7.1497209E-02 | 1.4932559E-01 | 7.0562025E-05 | 3.7846657E-02 | 7.3434750E-02 |
| 28.000 | 91.863 | 5.8595529E-02 | 1.2237977E-01 | 5.7829099E-05 | 3.1017223E-02 | 6.0183440E-02 |
| 29.000 | 95.144 | 4.8021960E-02 | 1.0029633E-01 | 4.7393832E-05 | 2.5420162E-02 | 4.9323332E-02 |
| 30.000 | 98.424 | 3.9356392E-02 | 8.2197847E-02 | 3.8841610E-05 | 2.0833091E-02 | 4.0422931E-02 |
| 31.000 | 101.705 | 3.2254526E-02 | 6.7365235E-02 | 3.1832636E-05 | 1.7073757E-02 | 3.3128608E-02 |
| 32.000 | 104.986 | 2.6434193E-02 | 5.5209170E-02 | 2.6088433E-05 | 1.3992795E-02 | 2.7150546E-02 |
| 33.000 | 108.267 | 2.1664141E-02 | 4.5246672E-02 | 2.1380774E-05 | 1.1467794E-02 | 2.2251227E-02 |
| 34.000 | 111.548 | 1.7754844E-02 | 3.7081904E-02 | 1.7522610E-05 | 9.3984299E-03 | 1.8235992E-02 |
| 35.000 | 114.829 | 1.4550981E-02 | 3.0390471E-02 | 1.4360654E-05 | 7.7024823E-03 | 1.4945305E-02 |
| 36.000 | 118.109 | 1.1925254E-02 | 2.4906505E-02 | 1.1769271E-05 | 6.3125685E-03 | 1.2248423E-02 |
| 37.000 | 121.390 | 9.7733414E-03 | 2.0412125E-02 | 9.6455060E-06 | 5.1734649E-03 | 1.0038194E-02 |
| 38.000 | 124.671 | 8.0097409E-03 | 1.6728755E-02 | 7.9049734E-06 | 4.2399126E-03 | 8.2268012E-03 |
| 39.000 | 127.952 | 6.5643822E-03 | 1.3710049E-02 | 6.4785200E-06 | 3.4748198E-03 | 6.7422738E-03 |
| 40.000 | 131.233 | 5.3798387E-03 | 1.1236069E-02 | 5.3094704E-06 | 2.8477882E-03 | 5.5256297E-03 |
| 41.000 | 134.514 | 4.4090462E-03 | 9.2085196E-03 | 4.3513758E-06 | 2.3339045E-03 | 4.5285292E-03 |
| 42.000 | 137.794 | 3.6134334E-03 | 7.5468413E-03 | 3.5661696E-06 | 1.9127512E-03 | 3.7113557E-03 |
| 43.000 | 141.075 | 2.9613889E-03 | 6.1850129E-03 | 2.9226539E-06 | 1.5675950E-03 | 3.0416411E-03 |
| 44.000 | 144.356 | 2.4270060E-03 | 5.0689267E-03 | 2.3952607E-06 | 1.2847223E-03 | 2.4927766E-03 |
| 45.000 | 147.637 | 1.9890525E-03 | 4.1542383E-03 | 1.9630356E-06 | 1.0528940E-03 | 2.0429547E-03 |
| 46.000 | 150.918 | 1.6301277E-03 | 3.4046054E-03 | 1.6088056E-06 | 8.6288923E-04 | 1.6743034E-03 |
| 47.000 | 154.199 | 1.3359710E-03 | 2.7902441E-03 | 1.3184964E-06 | 7.0718898E-04 | 1.3721752E-03 |
| 48.000 | 157.479 | 1.0948949E-03 | 2.2867442E-03 | 1.0805736E-06 | 5.7957665E-04 | 1.1245660E-03 |
| 49.000 | 160.760 | 8.9732103E-04 | 1.8741010E-03 | 8.8558407E-07 | 4.7499198E-04 | 9.2163800E-04 |
| 50.000 | 164.041 | 7.3539934E-04 | 1.5359193E-03 | 7.2578031E-07 | 3.8927962E-04 | 7.5532831E-04 |

| ALTITUDE (KM) | ALTITUDE (KF) | VELOCITY (KM/S) | VELOCITY (KF/S) | TIME FROM ENTRY (SEC.) |
|---|---|---|---|---|
| 0.000 | 0.000 | 8.9415150E-02 | 2.9335620E-01 | 6.3934973E+01 |
| 1.000 | 3.280 | 1.3545829E-01 | 4.4441606E-01 | 5.8275553E+01 |
| 2.000 | 6.561 | 1.9915457E-01 | 6.5339294E-01 | 5.4380182E+01 |
| 3.000 | 9.842 | 2.8455912E-01 | 9.3359103E-01 | 5.1616908E+01 |
| 4.000 | 13.123 | 3.9568338E-01 | 1.2981712E+00 | 4.9599415E+01 |
| 5.000 | 16.404 | 5.3616618E-01 | 1.7590718E+00 | 4.8085368E+01 |
| 6.000 | 19.684 | 7.0892207E-01 | 2.3258551E+00 | 4.6918960E+01 |
| 7.000 | 22.965 | 9.1580647E-01 | 3.0046083E+00 | 4.5997658E+01 |
| 8.000 | 26.246 | 1.1573404E+00 | 3.7970409E+00 | 4.5252470E+01 |
| 9.000 | 29.527 | 1.4325325E+00 | 4.6999003E+00 | 4.4635969E+01 |
| 10.000 | 32.808 | 1.7388200E+00 | 5.7047785E+00 | 4.4114883E+01 |
| 11.000 | 36.089 | 2.0721422E+00 | 6.7983531E+00 | 4.3665401E+01 |
| 12.000 | 39.369 | 2.4271372E+00 | 7.9630325E+00 | 4.3270136E+01 |
| 13.000 | 42.650 | 2.7974391E+00 | 9.1779313E+00 | 4.2916148E+01 |
| 14.000 | 45.931 | 3.1760486E+00 | 1.0420086E+01 | 4.2593600E+01 |
| 15.000 | 49.212 | 3.5557315E+00 | 1.1665762E+01 | 4.2294850E+01 |
| 16.000 | 52.493 | 3.9294108E+00 | 1.2891741E+01 | 4.2013827E+01 |
| 17.000 | 55.774 | 4.2905237E+00 | 1.4076493E+01 | 4.1745572E+01 |
| 18.000 | 59.054 | 4.6333076E+00 | 1.5201109E+01 | 4.1485920E+01 |
| 19.000 | 62.335 | 4.9510434E+00 | 1.6243548E+01 | 4.1232874E+01 |
| 20.000 | 65.616 | 5.2296130E+00 | 1.7157488E+01 | 4.0993149E+01 |
| 21.000 | 68.897 | 5.4695621E+00 | 1.7944721E+01 | 4.0765042E+01 |
| 22.000 | 72.178 | 5.6743988E+00 | 1.8616756E+01 | 4.0546035E+01 |
| 23.000 | 75.459 | 5.8479797E+00 | 1.9186246E+01 | 4.0334213E+01 |
| 24.000 | 78.739 | 5.9941897E+00 | 1.9665937E+01 | 4.0128101E+01 |
| 25.000 | 82.020 | 6.1167376E+00 | 2.0067996E+01 | 3.9926556E+01 |
| 26.000 | 85.301 | 6.2190375E+00 | 2.0403625E+01 | 3.9728678E+01 |
| 27.000 | 88.582 | 6.3041518E+00 | 2.0682871E+01 | 3.9533753E+01 |
| 28.000 | 91.863 | 6.3747750E+00 | 2.0914574E+01 | 3.9341217E+01 |
| 29.000 | 95.144 | 6.4332437E+00 | 2.1106400E+01 | 3.9150617E+01 |
| 30.000 | 98.424 | 6.4815614E+00 | 2.1264922E+01 | 3.8961587E+01 |
| 31.000 | 101.705 | 6.5214307E+00 | 2.1395727E+01 | 3.8773837E+01 |
| 32.000 | 104.986 | 6.5542882E+00 | 2.1503526E+01 | 3.8587128E+01 |
| 33.000 | 108.267 | 6.5813401E+00 | 2.1592279E+01 | 3.8401268E+01 |
| 34.000 | 111.548 | 6.6035937E+00 | 2.1665290E+01 | 3.8216101E+01 |
| 35.000 | 114.829 | 6.6218877E+00 | 2.1725309E+01 | 3.8031500E+01 |
| 36.000 | 118.109 | 6.6369183E+00 | 2.1774622E+01 | 3.7847361E+01 |
| 37.000 | 121.390 | 6.6492621E+00 | 2.1815120E+01 | 3.7663600E+01 |
| 38.000 | 124.671 | 6.6593955E+00 | 2.1848366E+01 | 3.7480149E+01 |
| 39.000 | 127.952 | 6.6677119E+00 | 2.1875651E+01 | 3.7296951E+01 |
| 40.000 | 131.233 | 6.6745353E+00 | 2.1898037E+01 | 3.7113960E+01 |
| 41.000 | 134.514 | 6.6801327E+00 | 2.1916401E+01 | 3.6931139E+01 |
| 42.000 | 137.794 | 6.6847235E+00 | 2.1931463E+01 | 3.6748456E+01 |
| 43.000 | 141.075 | 6.6884883E+00 | 2.1943815E+01 | 3.6565889E+01 |
| 44.000 | 144.356 | 6.6915752E+00 | 2.1953942E+01 | 3.6383413E+01 |
| 45.000 | 147.637 | 6.6941062E+00 | 2.1962246E+01 | 3.6201014E+01 |
| 46.000 | 150.918 | 6.6961812E+00 | 2.1969054E+01 | 3.6018678E+01 |
| 47.000 | 154.199 | 6.6978822E+00 | 2.1974634E+01 | 3.5836393E+01 |
| 48.000 | 157.479 | 6.6992767E+00 | 2.1979210E+01 | 3.5654150E+01 |
| 49.000 | 160.760 | 6.7004197E+00 | 2.1982960E+01 | 3.5471940E+01 |
| 50.000 | 164.041 | 6.7013566E+00 | 2.1986033E+01 | 3.5289760E+01 |

## C. Program Listing

### *1. The main program.*

```
C     LINEAR ENTRY-TRAJECTORY CALCULATIONS
C     MAIN PROGRAM
    1 FORMAT (8F10.0)
    2 FORMAT (6F10.0)
   11 FORMAT (24H SURFACE PRESSURE       =,F10.3,5H (MB))
   12 FORMAT (24H SURFACE DENSITY        =,F10.3,12H (E-05 G/CC))
   13 FORMAT (24H SURFACE TEMPERATURE    =,F10.3,8H (DEG.K))
   14 FORMAT (24H SURFACE GRAVITY        =,F10.3,10H (CM/SQ.S))
   15 FORMAT (24H SPECIFIC HEAT RATIO    =,F10.3)
   16 FORMAT (24H ADIABATIC LAPSE RATE   =,F10.3,11H (DEG.K/KM))
   17 FORMAT (24H TROPOPAUSE ALTITUDE    =,F10.3,5H (KM))
   18 FORMAT (24H INVERSE SCALE HEIGHT   =,F10.3,7H (1/KM))
   21 FORMAT (24HOENTRY ALTITUDE         =,F10.3,5H (KF))
   22 FORMAT (24H ENTRY VELOCITY         =,F10.3,7H (KF/S))
   23 FORMAT (24H ENTRY ANGLE            =,F10.3,10H (DEGREES))
   24 FORMAT (24H BALLISTIC COEFFICIENT  =,F10.3,13H (SLUGS/SQ.F))
   31 FORMAT (9H1ALTITUDE,4X,8HALTITUDE,8X,
     1         8HPRESSURE,11X,8HPRESSURE,11X,8HPRESSURE,12X,
     2         7HDENSITY,12X,7HDENSITY)
   32 FORMAT (7H   (KM),8X,4H(KF),12X,
     1         4H(MB),13X,8H(P/SQ.F),10X,10H(ATMSPHRS),9X,
     2         11H(E-05 G/CC),5X,17H(E-05 SLUGS/CU.F))
   33 FORMAT (1H0)
   34 FORMAT (F9.3,4X,F8.3,5X,
     1         1PE14.7,5X,1PE14.7,5X,1PE14.7,5X,
     2         1PE14.7,5X,1PE14.7)
   41 FORMAT (9H1ALTITUDE,4X,8HALTITUDE,8X,
     1         8HVELOCITY,11X,8HVELOCITY,8X,15HTIME FROM ENTRY)
   42 FORMAT (7H   (KM),8X,4H(KF),11X,
     1         6H(KM/S),13X,6H(KF/S),13X,6H(SEC.))
   43 FORMAT (F9.3,4X,F8.3,5X,1PE14.7,5X,1PE14.7,5X,1PE14.7)
      READ 1,PO,DO,TO,SG,SHR,ALR,HT,SHI
      READ 2,HE,VE,EA,BC,ALT,DELTA
      PRINT 11,PO
      PRINT 12,DO
      PRINT 13,TO
      PRINT 14,SG
      PRINT 15,SHR
      PRINT 16,ALR
      PRINT 17,HT
      PRINT 18,SHI
      SG=SG/100.
      PRINT 21,HE
      PRINT 22,VE
      PRINT 23,EA
      PRINT 24,BC
      HE=HE*.30480061
      VE=VE*.30480061
      BC=BC*157.08682
      EA=EA*.01745329
      CDV=2.*SG*BC*SINF(EA)
      CDT=SHI*VE*SINF(EA)
      PRINT 31
      PRINT 32
      PRINT 33
      H=0.
  103 CALL APDP(PO,DO,TO,SHR,ALR,HT,SHI,H,P,D)
      HC=H*3.2808333
      PC=P*2.0885514
      PA=P*.00098692
      DC=D*1.9403233
      PRINT 34,H,HC,P,PC,PA,D,DC
      IF (H-ALT) 101,102,102
  101 H=H+DELTA
      GO TO 103
  102 PRINT 41
      PRINT 42
      PRINT 33
      CALL APDP(PO,DO,TO,SHR,ALR,HT,SHI,HE,PE,DE)
      PE=PE*100.
      AE=PE/CDV
      CALL EIF(AE,EIE)
      H=0.
  203 CALL APDP(PO,DO,TO,SHR,ALR,HT,SHI,H,P,D)
      P=P*100.
      AVT=P/CDV
      V=VE*EXPF(-AVT)
      CALL EIF(AVT,EIT)
      T=(EIT-EIE)/CDT
      HC=H*3.2808333
      VC=V*3.2808333
      PRINT 43,H,HC,V,VC,T
      IF (H-ALT) 201,202,202
  201 H=H+DELTA
      GO TO 203
  202 STOP
      END
```

## 2. *The subroutines.*

```
      SUBROUTINE APDP(PO,DO,TO,SHR,ALR,HT,SHI,H,P,D)
C     ATMOSPHERIC PRESSURE/DENSITY PROFILE
      XPNTP=SHR/(SHR-1.)
      XPNTD=1./(SHR-1.)
      ARGT=1.+ALR*HT/TO
      PT=PO*ARGT**XPNTP
      PS=PT*EXPF(SHI*HT)
      DT=DO*ARGT**XPNTD
      DS=DT*EXPF(SHI*HT)
      IF (H-HT) 101,102,102
 101  ARG=1.+ALR*H/TO
      P=PO*ARG**XPNTP
      D=DO*ARG**XPNTD
      RETURN
 102  P=PS*EXPF(-SHI*H)
      D=DS*EXPF(-SHI*H)
      RETURN
      END
```

```
      SUBROUTINE EIF(X,EI)
C     EXPONENTIAL INTEGRAL FUNCTION
      EC=.5772156649
      XI=1.
      FCTRL=1.
      SUM=0.
 103  FCTRL=FCTRL*XI
      TERM=(X**XI)/(FCTRL*XI)
      SUM=SUM+TERM
      IF (TERM/SUM-1.E-08) 101,102,102
 101  EI=EC+LOGF(X)+SUM
      RETURN
 102  XI=XI+1.
      GO TO 103
      END
```

## References


1. Spencer, D. F., *Engineering Models of the Martian Atmosphere and Surface,* Technical Memorandum 33-234. Jet Propulsion Laboratory, Pasadena, Calif., July 1, 1965.

2. Spencer, D. F., "Our Present Knowledge of the Martian Atmosphere," paper presented at the AIAA meeting Stepping Stones To Mars, Baltimore, Md., Mar. 28, 1966.

3. Spencer, D. F., *An Evaluation of the Communication Blackout Problem for a Blunt Mars-Entry Capsule and a Potential Method for the Elimination of Blackout,* Technical Report 32-594. Jet Propulsion Laboratory, Pasadena, Calif., Apr. 15, 1964.

4. Ambrosio, A., "A General Atmospheric Entry Function and its Characteristics," *ARS J.*, pp. 906–910, June 1962.

5. Abraniowitz, M. and Stegun, I. A., *Handbook of Mathematical Functions,* National Bureau of Standards Applied Mathematics Series 55, U.S. Government Printing Office, Washington, D.C., pp. 227–251, June 1964.

6. Papas, C. H., *Theory of Electromagnetic Wave Propagation*, pp. 175–178. McGraw-Hill Book Co., Inc., New York, 1965.

7. Horton, T. E., *The JPL Thermochemistry and Normal Shock Computer Program,* Technical Report 32-660. Jet Propulsion Laboratory, Pasadena, Calif., Nov. 1, 1964.